C.E.D. Riboldi, S. Cacciola
Individual Pitch Control for 2-Bladed Wind Turbines via Multiblade Multilag Transformation
Wind Energy, Vol. 20, N. 12, 2017, p. 1955-1969
doi:10.1002/we.2133

WIND ENERGY
Wind Energ. 2017; **00**:1–16
DOI: 10.1002/we

RESEARCH ARTICLE

Individual pitch control for two–bladed wind turbines via multi–blade multi–lag transformation

C.E.D. Riboldi and S. Cacciola

Department of Aerospace Science and Technology, Politecnico di Milano, Milano, Via La Masa 34, 20156 Italy

ABSTRACT

Two–bladed wind turbines have regained the attention of the engineering community thanks to the advantages in manufacturing cost provided by the lower number of blades and the ease of implementation of effective passive systems for load reduction (i.e. teetering pin). Considering both teetering and non–teetering architectures, the dynamic response of two–bladed turbines is partly different from that of the more studied three–bladed machines, especially in terms of how multiples of the rotor frequencies in blade signals are translated on the fixed system. Such characteristics have hampered to a great extent the adoption of active control laws for load mitigation based on individual pitch control, extensively studied and validated for three–bladed turbines. Albeit some successful control solutions have been presented recently, a basic element for control development allowing to capture the essence of the relationship between signals on the blades and the fixed system on two–bladed turbines – represented by the Coleman transformation for three–bladed turbines – has not been identified yet. The present paper tries to fill the gap, presenting an extended transformation – called multi–blade multi–lag, or MBML – applicable to turbines with an arbitrary number of blades, and providing a systematic way to link rotor signals to fixed system signals, and allowing to successfully apply the well–known control algorithms for individual pitch control developed for three–bladed turbines to the two–bladed case. The paper addresses the problem in a first stage at a theoretical level, and subsequently providing applicative results from simulations on virtual models of teetering and non–teetering two–bladed turbines. The proposed transformation algorithm and control laws allow to effectively reduce some relevant loads and motions respectively in the non–teetering and teetering scenarios, by means of a cyclic pitch input.

KEYWORDS

Two–bladed rotors; individual pitch control (IPC); cyclic pitch; teetering; non–teetering; multi–blade transformation; multi–blade multi–lag (MBML) transformation

Correspondence

Carlo E.D. Riboldi, Department of Aerospace Science and Technology, Politecnico di Milano, Milano, Via La Masa 34, 20156 Italy.
E-mail: carlo.riboldi@polimi.it

Received . . .

1. INTRODUCTION

By now, it is widely accepted that the behavior of rotating blade systems, such as wind turbines or even helicopters, should be captured in a periodic framework rather than in a time invariant one. In fact, even in simple dynamic models of a rotating–wing system the characteristic coefficients feature a prominent periodic behavior [1, 2]. The fact that in steady conditions - i.e. also constant–in–time input - loads are time–periodic cannot be fully explained with the simpler linear time invariant (LTI) theory [3].

As a matter of fact, loads characterizing such systems, even in steady conditions, show a prominent periodic behavior, which should be carefully considered to avoid premature failures of components typically caused by fatigue. With the final aim of increasing machine life and designing cost-effective components, different techniques for load mitigation have been developed both for helicopters [4, 5] and three-bladed wind turbines based on the use of cyclic pitch [6, 7, 8, 9, 10, 11, 12, 13, 14, 15, 16]. An extensive overview of the current status of IPC application on three–bladed wind turbines is given in [17].

A specific difference between helicopter and wind turbine rotors lays in the separation between the rotor period and the time scales characterizing the inflow dynamics. For helicopters the flight dynamics is way slower than the rotor frequency and hence can be considered quasi–steady allowing the deployment of standard demodulation techniques, based on long data buffers. Conversely, for wind turbines the variation of the inflow induced by turbulence is in a frequency range comparable with the rotor frequency. This suggests that the extraction of periodic load components should be carried out with a minimum delay to avoid a too slow and inadequate control response[12].

For this reason, among the most widespread algorithms for wind turbines, the individual pitch control (IPC) proposed by Bossanyi and based on the Coleman (multi–blade) transformation has the advantage of a comparatively light scheme, bearing appreciable reductions on both blade and shaft loads with little effort in terms of design and implementation [8, 9, 10, 11, 15, 17].

The Coleman transformation, exploiting the instantaneous information provided by blade sensors, aims at promoting the 1P component of blade loads on three–bladed rotors to the constant value of the transformed loads, thus generating feedback signals which are easy to target by means of purely integral controllers. By suitably enlarging the usual Coleman transformation, it is possible to account for rotors with more than three blades.

On the other hand, by its very constitution, the transformation for two–bladed rotors cannot be written. As noted by some authors [18], deducing the expression of the Coleman transformation matrix for two–bladed rotors bears a singular result, where all frequency–promoting features of the transformation are lost.

Consequently, the problem of load mitigation for two–bladed rotors has received comparatively little attention from the community. The technical solution typically adopted by industry for reducing loads on two–bladed rotors, due to the unavailability of an accepted solution based on active control, consists in the addition of a teeter pin, basically changing the topology of the system by adding a new rigid degree of freedom. This has proven very effective for mitigating loads, at the non–negligible expense of a reduction in average power and power quality, and an increase in tip motion. Furthermore, loads coming from teeter end impacts may be highly significant on the envelope [19] and fatigue loads. From the viewpoint of design and certification these should be considered as relevant issues, especially when large rotors are of interest [20].

Concerning active control solutions, some authors [21, 22] recently proposed an ad–hoc alternative to the Coleman transformation for a two–bladed non–teetering rotor, producing a number of feedback control signals higher than the number of load inputs. The resulting controller is very sophisticated to design, considering multiple notch filters in conjunction with several complementary transformations. For teetering rotors an individual pitch control has been proposed in [23]. Here the teeter oscillation is targeted directly, but the implementation is again quite difficult to tune and based on multiple pass–band and notch filters. This may turn particularly critical for variable rotor speed as in turbulence.

In this work, a novel control scheme for two-bladed rotors is presented. The algorithm is based on a new transformation called multi–blade multi–lag (MBML), introduced by the authors in [24]. The basic idea of MBML is to exploit multiple samples of rotor signals recorded at predetermined azimuth angles in the past. By suitably choosing such lags it is possible to extract the harmonic amplitudes accurately and fast enough for load mitigation purposes. Furthermore, it will be shown that the MBML transformation bends itself to an implementation at higher harmonics, enabling a multi–frequency control. Finally, the architecture composed by MBML transformation and a suitable cyclic pitch control law, presented herein, can be applied satisfactorily in two slightly different ways, coping with both teetering and non–teetering turbines. For non–teetering rotors, the usual out–of–plane moments are targeted by the controller. In the case of teetering rotors, the teeter angle substitutes blade loads as a feed–back signal, leading to a combined passive and active control solution.

The present paper starts by recalling the multi–blade multi–lag (MBML) transformation and by declining it to the case of a two–bladed rotor. Thanks to the theoretical framework considered for its definition, the MBML transformation can be seamlessly written for rotors with an arbitrary number of blades, yielding easily predictable frequency–promoting characteristics. This makes such transformation suitable for producing control signals which can be effectively treated by means of integral or proportional–integral control laws. An application of a multi–frequency cyclic control based on this transformation, allowing to reduce several per–rev components of loads, will be shown on the virtual model of a two–bladed non–teetering turbine.

Subsequently, the paper takes into account a teetering configuration. A control algorithm able to reduce the teeter motion, while preserving the characteristics of load reduction typical to teetering rotors, will be presented. This topology and control architecture features schematic characteristics very similar to those described for the load–targeting control introduced for the non–teetering rotor, being again based on the MBML transformation.

Finally, a global comparison of all obtained results will be shown, helping in understanding the relative advantages and shortcomings of the considered controllers and two–bladed rotor configurations.

2. CYCLIC PITCH CONTROL VIA MULTI–BLADE MULTI–LAG TRANSFORMATION

As pointed out in the introduction, several implementations of cyclic control in the past have been based on the Coleman transformation. As noted in [18], this kind of transformation – which is a multi–blade transformation, as it makes use of

Wind Energ. 2017; **00**:1–16 © 2017 John Wiley & Sons, Ltd.
DOI: 10.1002/we
Prepared using weauth.cls

signals coming from all blades at the same time instant – is not defined for the case of two–bladed rotors. The problem can be tackled by considering the Coleman transformation as a special case of a wider family of transformations, called multi–blade multi–lag (MBML), based on the concept of considering for each time instant multiple azimuthal samples – the name multi–lag highlighting this – of the rotor signals.

The concept of the MBML transformation has been already introduced in [24], where, in conjunction with the cone coefficient [25], was used to design a control able to cope with aerodynamic imbalances. Here, MBML transformation will be recalled and specialized for the case of a two–bladed rotors, allowing an IPC control also for such systems. Afterward, the load–targeting control algorithm making use of the signals generated by the MBML will be presented.

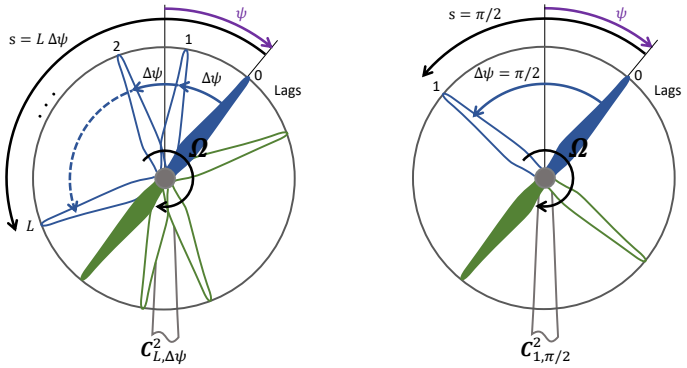

Figure 1. Sampling position examples for the multi–blade multi–lag transformation.

Figure 1 sketches on the left the basic idea of the MBML transformation for two–bladed rotors. Indeed, the two blade moments are not recorded only at the current azimuth ψ but also in one or more lagged positions $\psi - \ell\Delta\psi$, with $\ell = 1, \ldots, L$, where $\Delta\psi$ is the azimuthal sampling and L the total number of lags. Any MBML transformation is indicated with $\boldsymbol{C}^B_{L,\Delta\psi}$, being B the number of blades. As in this paper only two–bladed rotors are of our concern, the superscript B will be dropped.

Now it is clear that the number of data to exploit for extracting harmonic load components can be made as high as needed. Moreover, the azimuthal sampling $\Delta\psi$ and the number of lags L are to be chosen so as to ensure the performance required. The value $s = L\Delta\psi$ represents the support of the transformation: the lower the support is, the more the transformation is suited to being used for control purposes. On the right, blade configuration is displayed for the MBML transformation $\boldsymbol{C}_{1,\pi/2}$ (i.e. with $L = 1$ and $\Delta\psi = \pi/2$), which will be strongly employed throughout this paper.

2.1. Structure of the MBML transformation for a two–bladed rotor

Consider two generic signals – e.g. the out–of–plane moments – coming from the blades on a two–bladed rotor, sampled at the current azimuthal value of the rotor, corresponding to the two respective azimuth angles ψ_1 and ψ_2 of the blades. These signals can be stored in the array $\boldsymbol{m}(\psi) = \{m(\psi_1), m(\psi_2)\}^T$, where $\psi_2 = \psi_1 - \pi$ and $\psi_1 = \psi$, ψ being the rotor azimuth. In a strictly periodic condition, it is possible to fully describe $\boldsymbol{m}(\psi)$ based on its harmonic components as follows

$$\boldsymbol{m}(\psi) = \left\{ \begin{array}{c} a_0 + \sum_n a_{n,c}\cos(n\psi_1) + a_{n,s}\sin(n\psi_1) \\ a_0 + \sum_n a_{n,c}\cos(n\psi_2) + a_{n,s}\sin(n\psi_2) \end{array} \right\}. \tag{1}$$

We introduce now matrix $\boldsymbol{Q}(\psi)$, used in the next passages, as

$$\boldsymbol{Q}(\psi) = \left[\begin{array}{ccc} 1 & \cos(\psi_1) & \sin(\psi_1) \\ 1 & \cos(\psi_2) & \sin(\psi_2) \end{array} \right]. \tag{2}$$

Consider now another value of $\boldsymbol{m}(\psi)$ sampled at an azimuthal value shifted in the past by an angle $\Delta\psi$, which for now can be considered undetermined, stored in the array $\boldsymbol{m}(\psi - \Delta\psi) = \{m(\psi_1 - \Delta\psi), m(\psi_2 - \Delta\psi)\}^T$. Taking into account only the constant and 1P components in the signal, stacking together the current and shifted signals $\boldsymbol{m}(\psi)$ and $\boldsymbol{m}(\psi - \Delta\psi)$, it is easy to obtain the form

$$\left\{ \begin{array}{c} \boldsymbol{m}(\psi) \\ \boldsymbol{m}(\psi - \Delta\psi) \end{array} \right\} = \left[\begin{array}{c} \boldsymbol{Q}(\psi) \\ \boldsymbol{Q}(\psi - \Delta\psi) \end{array} \right] \left\{ \begin{array}{c} a_0 \\ a_{1,c} \\ a_{1,s} \end{array} \right\} + \boldsymbol{f} \tag{3}$$

where $\boldsymbol{f}$ conveys the contributions of all harmonics over the 1P.

Equation (3), expressing a general harmonic definition of the blade loads, can be inverted and used for estimating the harmonic amplitudes in the blade moments based on their respective measurements. It should be remarked that if lagged moments were not included – as in the case of the Coleman transformation –, the estimation synthesis could not be solved, i.e. the relationship could not be inverted due to the fact that there would be more unknowns – 3 harmonic amplitudes – than measurements – 2 moments. In this sense, the use of more lagged measurements, required by the MBML transformation algorithm, provides an effective tool to bypass a major obstacle posed by two–bladed rotors when trying to apply Coleman–based cyclic control.

From Equation (3) the harmonic estimation can be carried out through an inversion in a least–squares sense, yielding

$$\left\{ \begin{array}{c} a_0 \\ a_{1,c} \\ a_{1,s} \end{array} \right\}_{\mathrm{E}} = \left(\left[\begin{array}{c} \boldsymbol{Q}(\psi) \\ \boldsymbol{Q}(\psi - \Delta\psi) \end{array} \right]^T \left[\begin{array}{c} \boldsymbol{Q}(\psi) \\ \boldsymbol{Q}(\psi - \Delta\psi) \end{array} \right] \right)^{-1} \left[\begin{array}{c} \boldsymbol{Q}(\psi) \\ \boldsymbol{Q}(\psi - \Delta\psi) \end{array} \right]^T \left\{ \begin{array}{c} \boldsymbol{m}(\psi) \\ \boldsymbol{m}(\psi - \Delta\psi) \end{array} \right\} \tag{4}$$

where subscript E indicates estimated quantities. The estimation of the harmonic amplitudes at the 0P and 1P in Equation (4) will be polluted by higher harmonics in the moment signals. It can be seen that the polluting effect depends analytically on the value of $\Delta\psi$. This dependence can be exploited to relegate the disturbance to higher frequencies. As it will be clear from the proposed control algorithm, this characteristic of the MBML transformation provides the advantage of a wider separation between interesting lower frequencies and polluting frequencies in the controlled signals, which in turn allows to deploy low–pass filters with a wider band, thus reducing phase effects at lower frequencies.

In order to show how to practically select a suitable value of $\Delta\psi$, consider the estimation of the constant component $a_{0_{\mathrm{E}}}$, which can be obtained analytically inserting Equation (1) into (4) as

$$a_{0_{\mathrm{E}}} = a_0 + \frac{1}{2}a_{2,c}c_2 + \frac{1}{2}a_{2,s}s_2 + \frac{1}{2}a_{4,c}c_4 + \frac{1}{2}a_{4,s}s_4 + \dots \tag{5}$$

where $c_i = \cos(i\psi) + \cos(i(\psi - \Delta\psi))$ and $s_i = \sin(i\psi) + \sin(i(\psi - \Delta\psi))$. Looking at the shape of c_i and s_i it is apparent that in order to wipe out the polluting component at the 2P, $\Delta\psi$ must be equal to $\pi/2$. The resulting $a_{0_{\mathrm{E}}}$ writes

$$a_{0_{\mathrm{E}}} = a_0 + a_{4,c}\cos(4\psi) + a_{4,s}\sin(4\psi) - a_{8,c}\cos(8\psi) + a_{8,s}\sin(8\psi) + \dots \tag{6}$$

which features components at the 0P, 4P, 8P and higher harmonics. As stated above, thanks to the separation between the 0P and 4P, it will be possible to filter the polluting 4P frequency with a wide–band low–pass filter in order to preserve the constant component of interest – which in a realistic turbulent field scenario will be a slowly–varying, almost constant component – in the transformed signal.

A more complicated analytical relationship exists between the polluting harmonics and the estimated components at the 1P $a_{1,c_{\mathrm{E}}}$ and $a_{1,s_{\mathrm{E}}}$. The corresponding expressions, specialized for the case of $\Delta\psi = \pi/2$, yield

$$\begin{aligned} a_{1,c_{\mathrm{E}}} =& a_{1,c} + (a_{3,s}+a_{5,s})\sin(4\psi) + (a_{3,c}+a_{5,c})\cos(4\psi) + (a_{7,s}+a_{9,s})\sin(8\psi) + (a_{7,c}+a_{9,c})\cos(8\psi) + \dots \\ a_{1,s_{\mathrm{E}}} =& a_{1,s} + (a_{3,c}-a_{5,c})\sin(4\psi) - (a_{3,s}-a_{5,s})\cos(4\psi) + (a_{7,c}-a_{9,c})\sin(8\psi) - (a_{7,s}-a_{9,s})\cos(8\psi) + \dots \end{aligned} \tag{7}$$

It is possible to see from Equation (7) that both components feature the same harmonic content as the estimated constant value $a_{0_{\mathrm{E}}}$ in Equation (6), with different amplitudes. In particular, 3P and 5P on the blade are transferred to the 4P whereas the 7P and 9P are transferred to the 8P. Hence also in $a_{1,c_{\mathrm{E}}}$ and $a_{1,s_{\mathrm{E}}}$ the lowest polluting harmonic is at the 4P, similarly to $a_{0_{\mathrm{E}}}$.

A physical interpretation of setting the lag $\Delta\psi$ to $\pi/2$ is that the real two–bladed rotor has been augmented to a four–bladed rotor, with blades placed every 90 degrees, where the two real blades are flanked by two virtual ones. In strictly periodic operating conditions, the analogy would not imply any difference between a real and a pretended four–bladed rotor. When operating in the field, i.e. in a condition that is never strictly periodic, the signals coming from the two virtual blades at the current instant are simulated with those recorded from sensors on the real blades in the past, thus including a certain inaccuracy with respect to a real four–bladed rotor, with a level depending on how far from a periodic condition the rotor is actually working.

This last remark suggests that different MBML transformations, based on more than one lag in the past, could be used to emulate multi–bladed rotors with more than four blades. As an example, a MBML transformation with two lags may have a $\Delta\psi = \pi/3$, equivalent to a six–bladed rotor, whereas one with three lags may have a $\Delta\psi = \pi/4$, emulating an eight–bladed rotor, and so on. The higher the number of blades of the virtual rotor, the wider the separation between the desired and polluting frequencies in the transformed signals. On the other hand, simulating a rotor with a higher number of blades implies picking values of the signals recorded on the two real blades looking increasingly back in the past, hence introducing larger inaccuracies when working in the field – i.e. in not strictly periodic conditions.

Wind Energ. 2017; **00**:1–16
DOI: 10.1002/we
Prepared using weauth.cls

An explicit expression of the transform matrix for a $\Delta\psi = \pi/2$ can be finally obtained from Equation (4), as

$$\begin{Bmatrix} a_0 \\ a_{1,c} \\ a_{1,s} \end{Bmatrix}_{\mathrm{E}} = \begin{bmatrix} \frac{1}{4} & 0 & 0 \\ 0 & \frac{1}{2} & 0 \\ 0 & 0 & \frac{1}{2} \end{bmatrix} \begin{bmatrix} 1 & 1 & 1 & 1 \\ \cos(\psi_1) & \cos(\psi_2) & \cos(\psi_1 - \frac{\pi}{2}) & \cos(\psi_2 - \frac{\pi}{2}) \\ \sin(\psi_1) & \sin(\psi_2) & \sin(\psi_1 - \frac{\pi}{2}) & \sin(\psi_2 - \frac{\pi}{2}) \end{bmatrix} \begin{Bmatrix} m_1(\psi) \\ m_2(\psi) \\ m_1(\psi - \frac{\pi}{2}) \\ m_2(\psi - \frac{\pi}{2}) \end{Bmatrix} = \tag{8}$$

$$= \boldsymbol{T} \begin{bmatrix} \boldsymbol{Q}(\psi)^T & \boldsymbol{Q}(\psi - \frac{\pi}{2})^T \end{bmatrix} \begin{Bmatrix} \boldsymbol{m}(\psi) \\ \boldsymbol{m}(\psi - \frac{\pi}{2}) \end{Bmatrix} = \boldsymbol{C}_{1,\pi/2} \begin{Bmatrix} \boldsymbol{m}(\psi) \\ \boldsymbol{m}(\psi - \frac{\pi}{2}) \end{Bmatrix}$$

where $\boldsymbol{T} = \mathrm{diag}\{1/4,\ 1/2,\ 1/2\}$ and the MBML transformation matrix results to be $\boldsymbol{C}_{1,\pi/2} = \boldsymbol{T} \begin{bmatrix} \boldsymbol{Q}(\psi)^T & \boldsymbol{Q}(\psi - \frac{\pi}{2})^T \end{bmatrix}$. Finally, the support of this MBML is equal to $\pi/2$.

2.2. Multi–blade multi–lag transformation at higher harmonics

Until now, the formulation of the MBML transformation has been proposed focusing on the extraction of the 1P harmonics of blade signals. As it is the case with the Coleman transformation on three–bladed rotors, transformed loads can be fed back to a control law in order to mitigate both the 1P harmonic component of blade loads and equivalently the 0P in the nodding and yawing signals on the shaft.

However, it is well known that the harmonic content of the loads on the shaft is not limited to the 0P, nor the frequency spectrum of blade loads is limited to the 1P frequency – although this is the most prominent component. In order to reduce higher harmonic terms at the 2P, 4P, etc. on the shaft one has to extract also the higher harmonics (3P, 5P, etc.) present in the blade signals. To this end, it is possible to develop the MBML transformation at frequencies higher than the 1P, corresponding to the target frequencies on the blades.

The derivation process is similar to that presented above for the transformation operating at the 1P, redefining $\boldsymbol{Q}$ in Equation (2) as

$$\boldsymbol{Q}(n\psi) = \begin{bmatrix} 1 & \cos(n\psi_1) & \sin(n\psi_1) \\ 1 & \cos(n\psi_2) & \sin(n\psi_2) \end{bmatrix}. \tag{9}$$

where n represents the nP frequency where the transformation is intended to operate. The results previously obtained for $a_{0_{\mathrm{E}}}$, $a_{1,c_{\mathrm{E}}}$, and $a_{1,s_{\mathrm{E}}}$ in Equation (6) and (7) will be modified according to the transformation frequency of interest. Table (I) presents in a compact form the lowest residual frequency in the transformed signals as well as the lowest blade frequency amplitude contributing to the polluting terms of the transformed signals. Transformations corresponding to the 1P, 3P and 5P are considered, studying also the effect of using a shorter or more extended support s – i.e. a lower or higher number of virtual blades respectively given the value of $\Delta\psi$. The subscript $(\cdot)_{n_{L,\Delta\psi}}$ identifies the transformation matrix as operating at the nP frequency, with a number of lags (or virtual blades) L placed at an azimuthal distance $\Delta\psi$.

Table I. Characteristics of MBML transformations for 2–bladed rotors for different frequencies and lags.

	L	$\Delta\psi$ [deg]	s [deg]	Residual frequency	Lowest blade bearing frequency
$\boldsymbol{C}_{1_{1,\pi/2}}$	1	90	90	4×Rev	3×Rev
$\boldsymbol{C}_{1_{2,\pi/3}}$	2	60	120	6×Rev	5×Rev
$\boldsymbol{C}_{1_{3,\pi/4}}$	3	45	135	8×Rev	7×Rev
$\boldsymbol{C}_{3_{1,\pi/2}}$	1	90	90	4×Rev	2×Rev
$\boldsymbol{C}_{3_{2,\pi/3}}$	2	60	120	Singular	
$\boldsymbol{C}_{3_{3,\pi/4}}$	3	45	135	8×Rev	6×Rev
$\boldsymbol{C}_{5_{1,\pi/2}}$	1	90	90	4×Rev	1×Rev
$\boldsymbol{C}_{5_{2,\pi/3}}$	2	60	120	6×Rev	1×Rev
$\boldsymbol{C}_{5_{3,\pi/4}}$	3	45	135	8×Rev	3×Rev

As a first remark to Table (I) it can be noticed that no transformation at the 2P and 4P have been accounted for, for these would be singular as it is the case for higher harmonic Coleman transformations at the 3P or 6P for three–bladed rotors. Moreover, a blade motion at the 2P, 4P, *etc.* results in a collective rather than a cyclic pitch action. Furthermore, certain combinations of frequency of the transformation, number of virtual blades and value of the azimuth lag generate singular transformations, as it is the case for $\boldsymbol{C}_{3_{2,\pi/3}}$.

Another remark is related to the values of the lowest harmonic amplitude in the polluting signal, reported on the rightmost column on the table. It should be observed that, depending again on the settings of the MBML transformation, the harmonic amplitude of the blade signal transferred to the lowest polluting frequency of the transformed signal may

correspond to largely different frequencies. As an example, the amplitude of the 6P on the blades, which will be transferred at the 8P disturbance in the transformed signals when $\boldsymbol{C}_{3_{3,\pi/4}}$ is used, will be much lower in intensity with respect to the 1P of the blades signal, transferred to the 4P in the transformed signals when $\boldsymbol{C}_{5_{1,\pi/2}}$ is used. Considering blade out–of–plane loads and the usual amplitudes of the 1P and 6P in them, this effect makes the low–pass filtering action an urgent necessity and a delicate task especially for the case of the $\boldsymbol{C}_{5_{1,\pi/2}}$ transformation. Luckily, as already stated and again clearly apparent from Table (I), the MBML transformation allows a wide separation between the constant – or slowly varying – components and the polluting harmonics in the spectra of transformed signals, thus imposing a more limited phase–effect.

2.3. Control via MBML–transformation

The ability of the MBML transformation to select some components of the frequency content of blade loads, and more in general of blade–related quantities – promoting them to constant values, at least in strictly periodic conditions – can be exploited similarly to the case of the Coleman transformation for three–bladed rotors to target such harmonic components via a suitable control system [8, 12, 13, 15].

The transformation matrices derived in the previous paragraphs allow to apply to the case of two–bladed rotors a control scheme mostly similar to that developed and extensively studied for three–bladed turbines. The proposed implementation is based on the multi–layer paradigm [12], where an load–targeting control loop produces a cyclic pitch signal $\boldsymbol{\beta}^{cyc}$, to be added up to the collective pitch signal $\boldsymbol{\beta}^{\mathrm{COL}}$ produced along with the generator torque by a trimming loop. The two control layers are designed separately, and here we focus only on the layer for cyclic pitch control.

Considering an application with a MBML transformation working at the 1P only, in the proposed scheme the signals sampled on the two blades at the current azimuth, as well as at the required azimuth values in the past, composing the array of measurements $\boldsymbol{m}(\psi) = \{m(\psi), m(\psi - \pi/2)\}$, are fed to the MBML transformation $\boldsymbol{C}_{1_{1,\pi/2}}$. Of the resulting three output signals (as from Equation (8)), amplitudes $a_{1,c_{\mathrm{E}}}$ and $a_{1,s_{\mathrm{E}}}$ are responsible for the constant values of shaft nodding and yawing moments, and they can be targeted by means of a cyclic pitch control operating at the 1P.

Before being fed to the control laws, these two amplitudes are treated with low–pass filters. These wipe out all polluting harmonic components, while keeping the constant – and the lowest–frequency section of the spectrum – to its correct value. The wide frequency separation between the low frequency values of interest and the first polluting component provided by the MBML transformation can be fully exploited here to avoid relevant phase effects, otherwise connected with the filtering action.

The so–obtained transformed and filtered signals are passed to a phase compensator to correct for the system dynamics lag [8, 9]. Such phase compensator needs to be scheduled with respect to the wind speed, for the intensity of the phase lag effect may be different over the operating envelope of the turbine. The resulting signals are received by two PI controllers, producing two pitch control signals. The process is analytically described in Equation (10), yielding

$$\boldsymbol{\beta}_1 = \left\{ \begin{array}{c} \beta_{1,c} \\ \beta_{1,s} \end{array} \right\} = \left[\begin{array}{c} k_P^1(\cdot) + k_I^1 \int(\cdot)\mathrm{d}t \\ k_P^2(\cdot) + k_I^2 \int(\cdot)\mathrm{d}t \end{array} \right] \boldsymbol{P}(V_m) \left\{ \begin{array}{c} a_{1,c} \\ a_{1,s} \end{array} \right\}_{\mathrm{E}} \tag{10}$$

where $\boldsymbol{P}$ is a 2–by–2 rotation matrix correcting for the phase effect and is a function of the rotor average wind speed V_m, estimated from a filtered measure from an anemometer on top of the tower or retrieved from an ad–hoc optimal observer based on torque balance equation [17]. The latter solution is the mostly adopted by industry.

Finally, the control signals $\boldsymbol{\beta}_1 = \{\beta_{1,c},\, \beta_{1,s}\}^T$ can be modulated at the 1P providing the required cyclic control input to be summed up to the collective value coming from the trimmer and eventually sent to the actuators. The modulating matrix writes

$$\boldsymbol{M}(\psi) = \left[\begin{array}{cc} \cos(\psi_1) & \sin(\psi_1) \\ \cos(\psi_2) & \sin(\psi_2) \end{array} \right], \tag{11}$$

such that $\boldsymbol{\beta}_1^{cyc} = \boldsymbol{M}(\psi)\boldsymbol{\beta}_1$.

Figure 2 synthetically illustrates the control scheme.

It should be remarked that there is no *a priori* restriction concerning the choice of the blade signals to be fed to the transformation. As stated in the introduction, in this paper we present two applications of the proposed control scheme, coping with the dynamics of either non–teetering and teetering rotors.

The dynamics of a non–teetering two–bladed rotor is qualitatively similar to that of a three–bladed rotor, hence for that case the out–of–plane loads measured at the root of the blades can be selected as target signals to be controlled. In this scenario, the control system is expected to reduce the loads on the blades and on the shaft by means of a cyclic control action.

The dynamics of a teetering rotor is governed by the effect of the teeter degree of freedom, which is very effective in reducing blade and shaft bending loads, at the expense of a potentially relevant fore–aft displacement of blade tips. For this kind of rotor it is possible to exploit the proposed control algorithm considering the teeter angles of the two blades – which will be clearly one the opposite of the other – as controlled variables, instead of load signals. As it will be apparent from

DOI: 10.1002/we
Prepared using weauth.cls

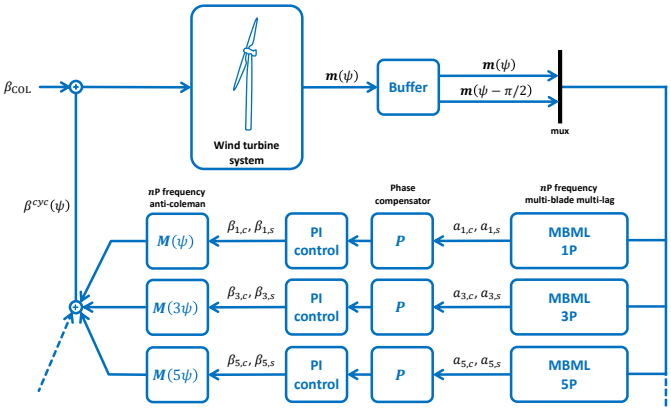

Figure 2. Architecture of the MBML–based control.

the results, this control architecture proves very satisfactory in reducing tip displacements, a relevant quantity in terms of design and certification, while also further reducing oscillating loads on the blades and shaft with respect to a teetering rotor with no cyclic control.

Both control architectures are represented by the scheme in Figure 2, the meaning attributed to the generic signal collected in $\boldsymbol{m}(\psi)$ being the only distinctive feature of those control problems.

Two differences between the two scenarios just introduced should be accounted for when it comes to practically designing the corresponding cyclic pitch controllers. Firstly, the frequency content of loads on the blades for a non–teetering rotor will feature components at all multiples of the per–rev frequency, the lowest two to four frequencies usually contributing with the same order of magnitude. On the other hand, the frequency spectrum of the teeter angle features contributes at the 1P, 3P, 5P and so on, but with the 1P being by far the most prominent components of all. For this reason, for the non–teetering scenario it makes sense to operate a multi–frequency cyclic control working at the 1P as well as at the 3P, 5P and potentially higher frequencies, whereas for the teetering rotor operating a cyclic control at the 1P provides already an advantage in performance sufficiently close to the top attainable. Considering Figure 2, only the cyclic controller at the 1P frequency is operating, and all those at higher harmonics are deactivated. Secondarily, the dynamics of the teetering rotor produces a response of blade–related quantities – including the teeter angle – which is lagged by an azimuth of $\pi/2$ with respect to the control action. For this reason, in the case of teetering rotors, scheduling of the phase compensator is not necessary, and matrix $\boldsymbol{P}$ in Equation (10) will be constant with V_m.

Considering the application of the cyclic pitch controller to non–teetering rotors, in case targeting harmonic components higher than the 1P on blade loads is of interest, it is possible to replicate the control algorithm based on a MBML transformation working at a higher frequency nP, with $n = 3, 5, \ldots$.

The information contained in the lowest part of the spectrum of the transformed signals $a_{n,c_{\mathrm{E}}}$ and $a_{n,s_{\mathrm{E}}}$ below the first polluting frequency (see Table (I)) can be extracted with mild low–pass filters. For each transformation frequency n, a phase compensator represented by $\boldsymbol{P}_n$, can be used to account for the lag between the nP frequency in the target signal and the same frequency in the pitch input signal, and to take care of the correct phasing of control. Compensating for the phase effect becomes more and more relevant for increasing nP frequencies. The control law will be formally similar to that written for the 1P frequency loop (Equation (10)), and its output $\boldsymbol{\beta}_n$ will be transformed back into two cyclic components in time through a modulation at the frequency of the transformation represented by matrix $\boldsymbol{M}(n\psi)$, obviously defined from Equation (11).

The contributions coming from the control layers at all frequencies are summed up together and added to the collective input, before being fed to the actuators.

3. RESULTS

The control laws presented in the previous sections for both the teetering and non–teetering configurations have been extensively tested in virtual environment. The model of a two–bladed 550 kW turbine, largely based on the CART2 testbed [18], has been implemented in FAST [26], with minor modifications concerning the power set–point and blade aerodynamics, as well as mass and stiffness distributions. For an easier comparison of the results, the teetering and non–teetering models differ only for the activation of the teeter degree of freedom. Even though from a design standpoint this

might be a questionable choice, as some key components of the turbine like the blade and drive-train may be designed differently for teetering or non–teetering rotors, the maximum commonality between the considered test turbines has been privileged to better highlight the difference in load abatement performance due to the teeter degree of freedom and to the cyclic pitch control laws.

All flexible degrees of freedom on tower and blades allowed by FAST have been accounted for [26]. Control routines have been implemented in a tree of dynamically linked libraries, interfaced with FAST through a communication library, where also actuator and sensor dynamics have been included. Both pitch and torque actuators have been modeled as first order systems. In all considered simulations the machine is kept trimmed at the correct power output for each wind speed by means of the same LQR trimmer, governing the value of collective pitch and torque [27]. The controllers for cyclic pitch produce pitch input signals which are added to the collective value in a multi–layer fashion before being fed to the actuators [12, 13].

The results are presented in three parts. The first is focused on the use of a multi–frequency cyclic pitch controller based on the MBML transformation and the feedback of blade loads on a non–teetering rotor. The second part is centered on the application of a MBML transform–based cyclic control to the case of a teetering configuration, where the target feedback variable is the teeter angle. In both sections a quantitative analysis in time or frequency domain on some example simulations will be proposed, trying to show the effect of the compared controls. Finally, a comparison of all configurations and control schemes will be presented in a more comprehensive framework, showing the relative advantages over the operational wind range of the turbine.

3.1. Multi–blade multi–lag control of a non–teetering rotor

In the case of the non–teetering configuration, a comparison between a reference condition where only the trimmer is working and one where both the trimmer and cyclic pitch controller are active will be presented.

The control algorithm is fed with the out–of–plane loads from the two blades, sampled at the current azimuth as well as at $-\pi/2$ into the past. These four values are fed back instantly to the MBML transformation previously shown for each assigned transformation frequency. The resulting two signals are low–pass filtered with a fourth–order Butterworth filter with a cut–off frequency slightly above the 1P, and turned over to a coupled proportional–integral controller producing two equivalent pitch control signals. These are transformed back via the inverse transformation corresponding to the assigned frequency, and finally added up to the collective control value from the underlying trimmer.

The same procedure can be applied at several frequencies of interest by simply replicating the scheme above accounting for a transformation matrix suitably defined at that very frequency. The pitch control inputs from all the loops corresponding to the various frequencies will be summed up, and added to the collective control input before being fed to the actuators.

The gains of the PI can be tuned for just one frequency and then used for the others, for the control loops corresponding to all considered frequencies will be targeting low–pass filtered transformed signals, where the most relevant frequency component – in ideal wind conditions, the only one – to be lowered will be the constant. This allows deploying a gain optimization technique for cyclic control gains conceived for a single frequency loop [16], and then applying the so–optimized gains to all frequencies.

As stated above, the PI controllers will be coupled due to the phase effect resulting from the dynamics of actuators. As a consequence, the cosine and sine components of the transformed loads will not be targeted only by means of cosine and sine pitch components respectively. The quantification of the phase needed for correctly tuning the PI loops can be carried out preliminarily by exciting the system – with only the trimmer running – with a cosine and sine cyclic pitch input at the frequency of interest, and by studying the cosine and sine response of the transformed loads, obtained from the MBML transformation again at the frequency of interest. The phase effect is a function of wind, with a very strong gradient especially in partial power region, but a non–null gradient also over the span of the full power region, as shown in Fig. 3. This feature of the problem can be coped with by adopting a scheduled control, where a phase correction is properly accounted for through a suitable pre–computed transformation, where the coefficients are a function of the measured wind speed.

In Figure 4 the results of a simulation in constant, vertically sheared wind of 19 m/sec intensity is presented. The plots correspond to the nodding and yawing bending measured on the shaft at the level of the hub, to the out–of–plane bending at the root of the first blade, and to the pitch of the same blade.

The outcome corresponding to simulation runs with the cyclic controller acting at different frequencies are reported together. Cases where the controller is operating at the 1P, at the 1P and 3P and finally at the 1P, 3P and 5P are all presented and compared to the reference condition where the trimmer is working alone.

Looking at the nodding and yawing signals, the results show that a large improvement on both can be obtained by the cyclic controller working at the 1P, especially in terms of the constant values. A further improvement can be obtained at higher frequencies by adding control components at the 3P and 5P. Differences with respect to the reference in the loads

DOI: 10.1002/we
Prepared using weauth.cls

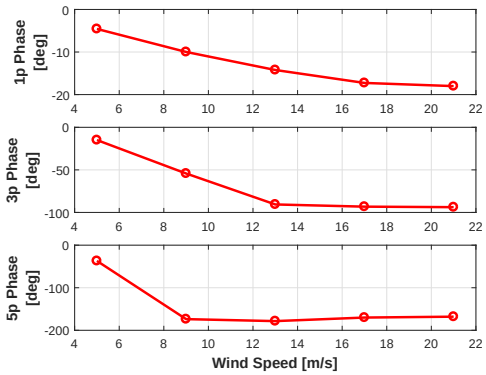

Figure 3. Behavior of the phase lag as a function of the wind speed. The three subplots show the phase between the demanded pitch and out–of–plane bending moment at the 1P, 3P and 5P components respectively from top to bottom.

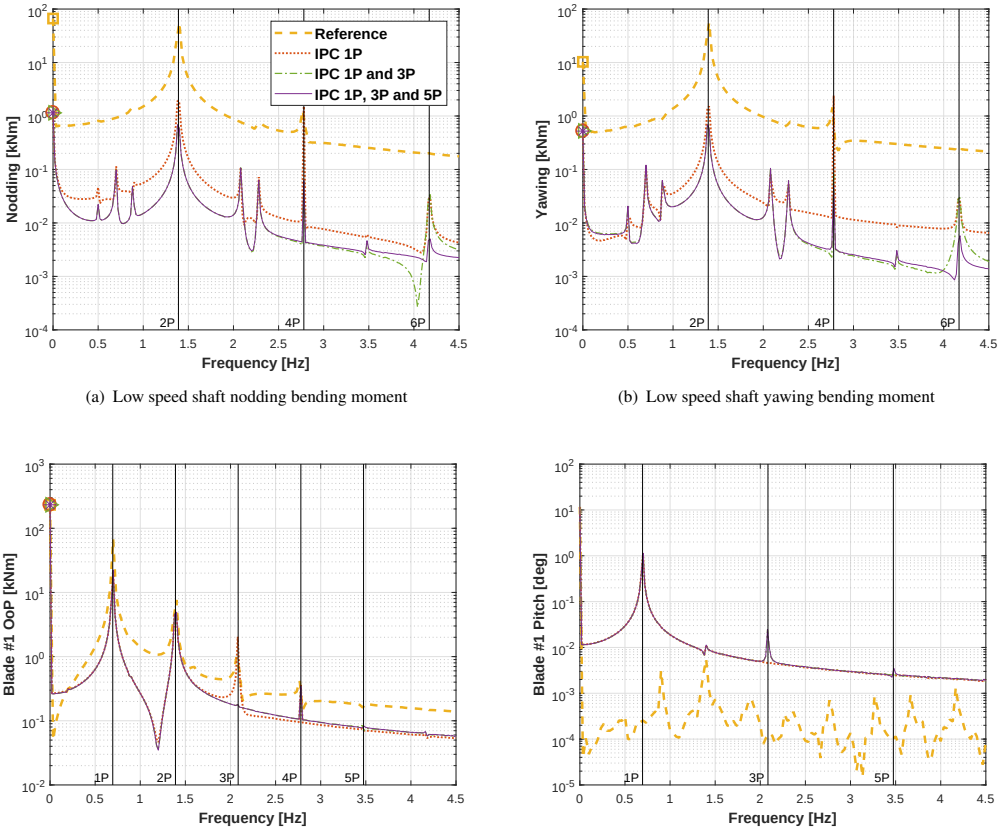

(a) Low speed shaft nodding bending moment

(b) Low speed shaft yawing bending moment

(c) Blade 1 out of plane bending moment

(d) Blade 1 pitch angle

Figure 4. Frequency spectra of nodding (a), yawing (b), out–of–plane bending moment (c) and pitch (d) of nr.1 blade from 150 sec simulations in NWP at 19 m/sec. Yellow dashed: reference (no cyclic pitch). Red dotted: cyclic operating at 1P. Green dash–dotted: cyclic operating at 1P and 3P. Purple solid: cyclic operating at 1P, 3P and 5P.

tend to be more reduced at higher frequencies, so controlling at frequencies higher than the 3P, responsible for reductions at the 4P and 6P in the loads, would not imply significant further advantages.

From plot (c) on Figure 4 it is possible to notice that cyclic pitch is as expected very beneficial on the out–of–plane load. All advantages come at the price of a higher motion of pitch actuators, reflected by a visible increase in pitch motion at the considered frequencies of actuation.

Figure 5 shows results of the power spectral density obtained from a 600 sec run in 19 m/sec average A category (Cat. A) turbulence [28] for the same control scenarios considered in Figure 4. Based on the fact that no increase of the targeted quantities is apparent, it can be concluded that turbulence is not a critical factor for control performance. The same remark made for the constant wind case apply, and it should be noted that also advantages due to passing from a 1P and 3P to a 1P, 3P and 5P actuation are not very large, further indicating that moving to a multi–frequency control architecture at input frequencies higher than the 3P is not necessary.

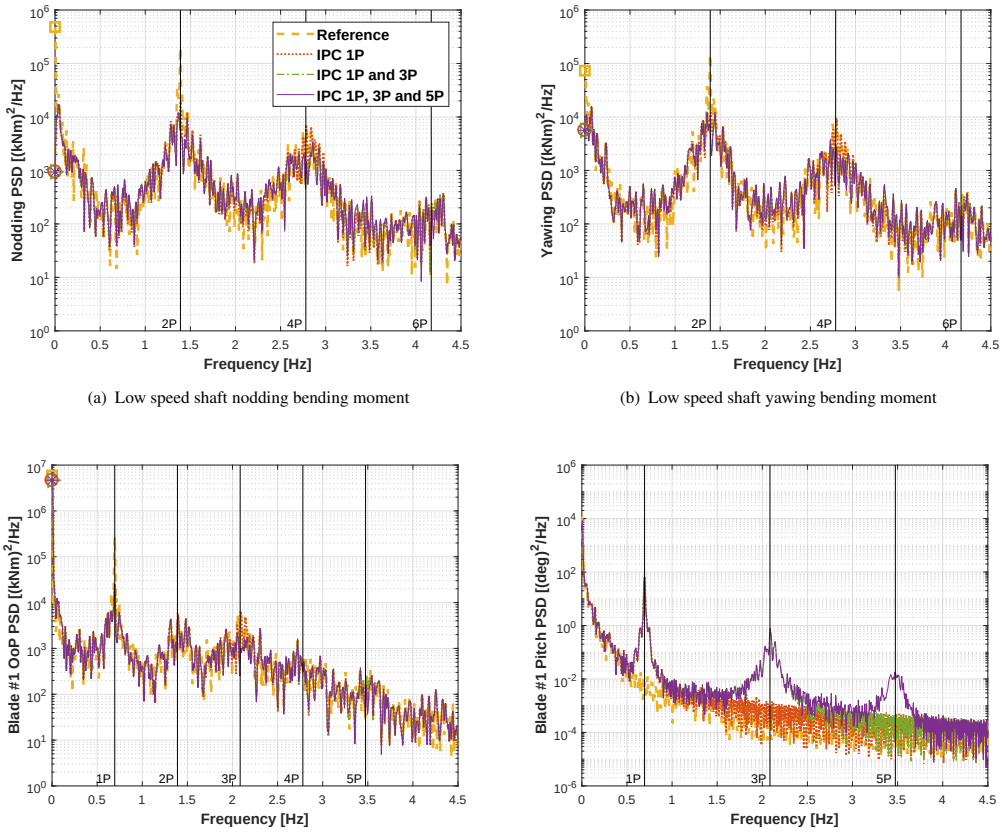

(a) Low speed shaft nodding bending moment

(b) Low speed shaft yawing bending moment

(c) Blade 1 out of plane bending moment

(d) Blade 1 pitch angle

Figure 5. Power spectral density of nodding (a), yawing (b), out–of–plane bending moment (c) and pitch (d) of nr.1 blade from 600 sec simulations in Cat. A turbulence with an average wind intensity of 19 m/sec. Yellow dashed: reference (no cyclic pitch). Red dotted: cyclic operating at 1P. Green dash–dotted: cyclic operating at 1P and 3P. Purple solid: cyclic operating at 1P, 3P and 5P.

3.2. Multi–blade multi–lag control of a teetering rotor

As explained above, the MBML–based cyclic controller proposed for the teetering configuration takes as input the teeter angle of the blades instead of the out–of–plane moments as it is the case for the non–teetering configuration. The formulation of control is mainly the same as for the case of the non–teetering configuration. Two teeter angle signals, referring to the two blades, are obtained from a single actual measure, for the teeter angles of the two signals are by definition one the opposite of the other. Similarly to the non–teetering case, the MBML is based on samples at the actual azimuth and at $\pi/2$ radians in the past. The resulting set of four samples is transformed obtaining two signals, which are passed to a coupled PI control law after low–pass filtering.

A similar remark as for the non–teetering case applies here concerning phase. Differently from before, phase does not change significantly with wind speed, and it is very close to $\pi/2$. This is bound to the fact that the frequency of the free teeter mode is exactly equal to the rotor frequency. For this reason, a cyclic pitch input at the 1P frequency produces an

Wind Energ. 2017; **00**:1–16 © 2017 John Wiley & Sons, Ltd.
DOI: 10.1002/we
Prepared using weauth.cls

effect on teeter motion delayed by a phase of $\pi/2$ – in other words, the teeter motion is in resonance with respect to the 1P cyclic control in any operating condition. The exact value of the phase delay can be altered typically by two effects, namely a teeter hinge which is not fully free, but constrained by a concentrated equivalent stiffness, or actuator dynamics. In the present case the hinge is fully free, whereas the fast actuator dynamics does not bring in any significant alteration to the phase of the response. However, similarly to the non–teetering case, any delay in the response can be accounted for by simply changing the value of the phase, possibly scheduled with respect to the wind, without modifying the architecture of the controller.

The lack of further practical improvements when operating cyclic pitch at frequencies higher than the 1P has led to the adoption of a single–frequency cyclic control, differently from the case of the non–teetering configuration presented above.

Figure 6 presents a comparison of the time histories of the teeter angle, blade 1 pitch nodding and yawing bending moments on the shaft at the level of the hub, and of the pitch input of the first blade. for the reference case of a teetering configuration with only the trimmer working and for a scenario where the MBML–based cyclic control is active at the 1P. The scenario refers to a constant, sheared wind of 19 m/sec. The result shows a remarkable reduction of the teeter angle and of both considered loads.

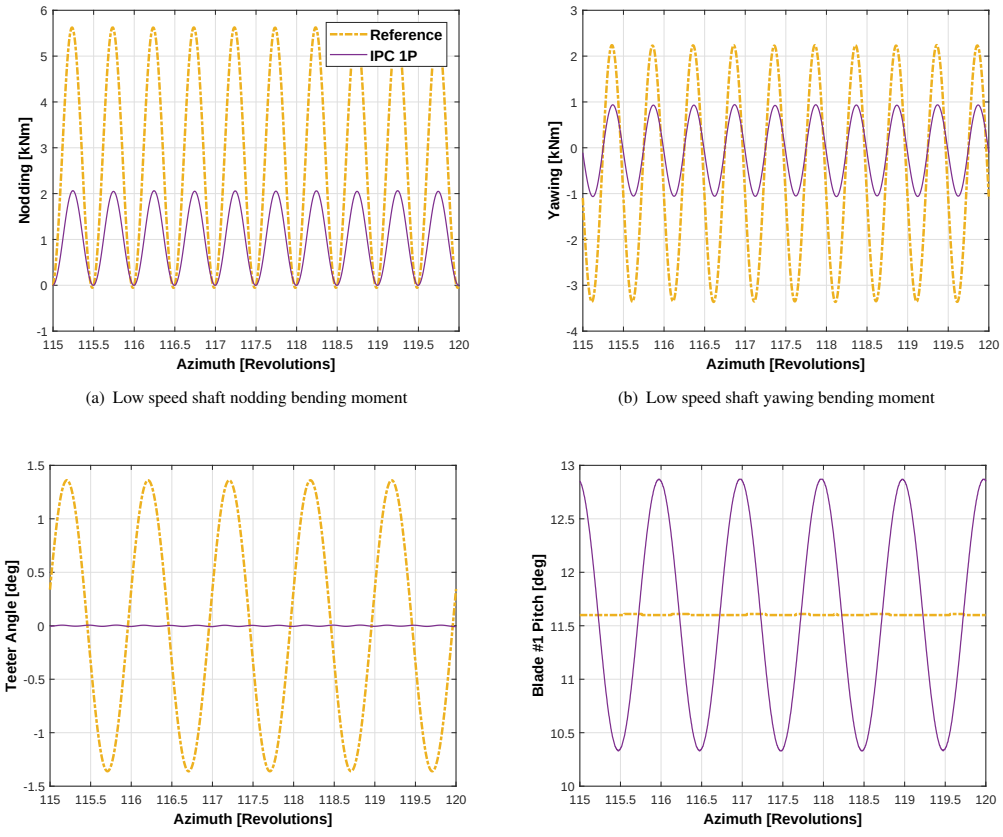

(a) Low speed shaft nodding bending moment

(b) Low speed shaft yawing bending moment

(c) Teeter angle

(d) Blade 1 pitch angle

Figure 6. Time histories of nodding (a), yawing (b), teeter angle (c) and nr.1 blade pitch (d) from 150 sec simulations in NWP at 19 m/sec. Yellow dash–dotted: reference (no cyclic pitch). Purple solid: cyclic operating at 1P.

Results in Cat. A turbulence tend to confirm those obtained in constant wind. Figure 7 shows the outcome in terms of power spectral density of the teeter angle, blade 1 pitch and both nodding and yawing moments on the shaft, for 600 sec simulation with an average wind speed of 19 m/sec.

3.3. Comparison of configurations and control schemes

For a comprehensive comparison of both non–teetering and teetering configurations, and the corresponding cyclic controllers, the model turbine has been subjected to 600 sec turbulent wind histories with average speeds of 5 to 21 m/sec

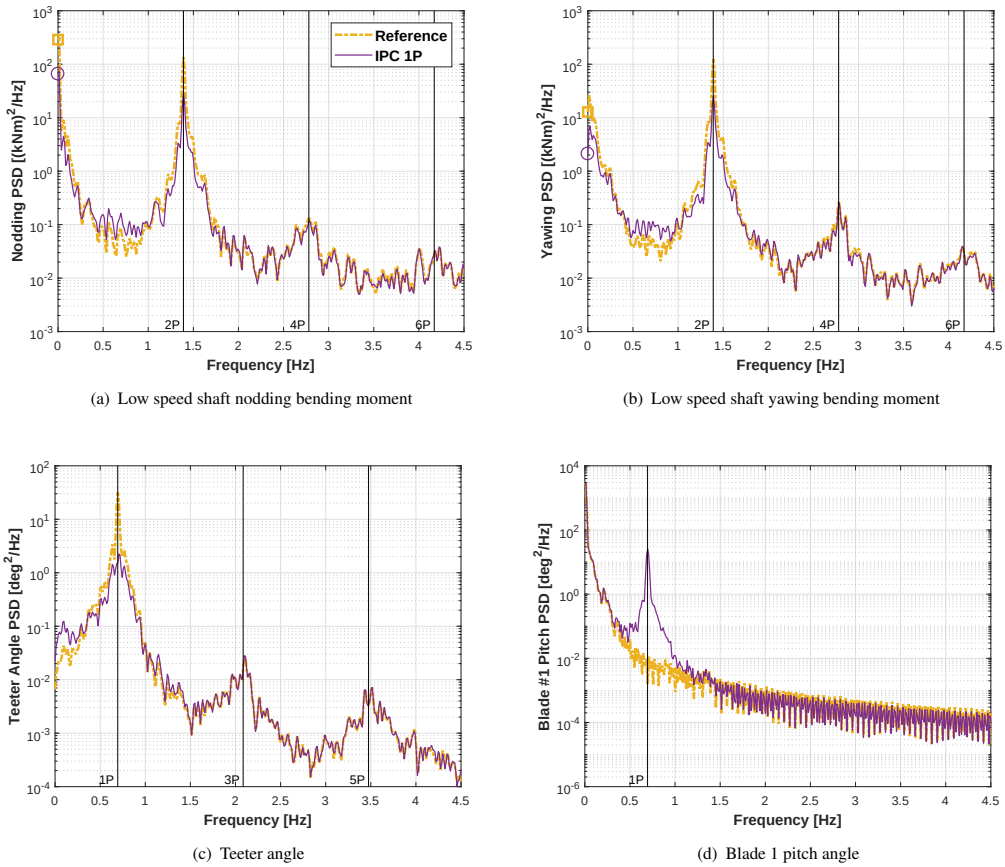

(a) Low speed shaft nodding bending moment

(b) Low speed shaft yawing bending moment

(c) Teeter angle

(d) Blade 1 pitch angle

Figure 7. Power spectral density of nodding (a), yawing (b), teeter angle (c) and nr.1 blade pitch (d) from 600 sec simulations in Cat. A turbulence at 19 m/sec average wind speed. Yellow dash–dotted: reference (no cyclic pitch). Purple solid: cyclic operating at 1P.

every 4 m/sec, and an 8% turbulence intensity. Concerning loads, the performance has been analyzed in terms of damage equivalent load (DEL) of the out–of–plane moment at the root of the first blade, and of the nodding and yawing moments on a cross section of the shaft at the level of the hub. Further quantities of interest are average power output and relative standard deviation, and maximum blade tip motion in the direction of the rotor axis.

All figures in this section have the average wind speed on the horizontal axis, and for each wind speed the plots present groups of four columns, referring from left to right to a reference non–teetering condition with no cyclic control, a non–teetering configuration with a multi–frequency MBML–based cyclic control working on transformed out–of–plane loads, with pitch operating at the 1P, 3P and 5P as in Subsection 3.1, a teetering configuration with no cyclic control, and finally a teetering configuration with an MBML–based cyclic control working on teeter angle, as in Subsection 3.2.

Plots on Figure 8 report the results for nodding and yawing. These two–scale plots clearly show that a significant improvement in shaft loads can be obtained from the adoption of a teetering configuration (two rightmost columns in each group) with respect to a non–teetering one. On the other hand, as it was anticipated in Subsection 3.1, a relevant load–mitigating effect can be obtained in a non–teetering configuration when applying the proposed control algorithm. Considering the non–teetering configuration with cyclic control, it should be remarked that when analyzing the performance on an array of winds spanning from the cut–in to close to the cut–out, accounting for the changing phase of the controller with respect to the wind is necessary. For this reason, as highlighted in Subsection 3.1 a scheduling was implemented in the tested control configuration, where phase values are linearly interpolated based on a moving–average–filtered value of the wind speed between nodal values assigned for five wind speeds scattered over the operational envelope.

This issue does not show up so evidently in the case of the teetering rotor, where the phase between pitch and teeter motion signals is very close to $\pi/2$ all over the operating envelope of the machine thus making scheduling unnecessary.

Wind Energ. 2017; **00**:1–16 © 2017 John Wiley & Sons, Ltd.
DOI: 10.1002/we
Prepared using weauth.cls

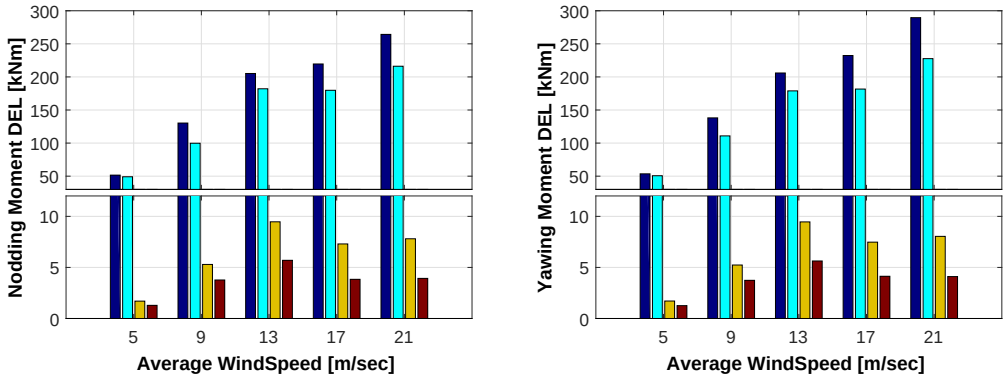

(a) Low speed shaft nodding bending moment

(b) Low speed shaft yawing bending moment

Figure 8. Nodding (a) and yawing (b) DEL as functions of wind intensity, computed from 600 sec simulations with turbulence intensity 8%. Columns from left to right: non–teetering reference control, non–teetering with multi–frequency MBML–based cyclic, teetering with reference control, teetering with cyclic control on teeter angle.

Load reductions due to cyclic control tend to be smaller at lower speeds on both rotors. The superiority of the teetering configuration in this performance can be noticed also looking at the behavior of the considered loads for increasing wind speeds. Considering the cases where no cyclic control is active, loads are generally increasing for the non–teetering configuration, whereas they reach a maximum close to the rated, settling to a somewhat lower value at the highest considered speeds for the teetering case.

Considering the out–of–plane bending measured at the root of the blade, from the comparison in Figure 9 the result is again rather different between the non–teetering configuration and the teetering one, with generally higher loads on the non–teetering rotor, which also tend to increase with the wind speed.

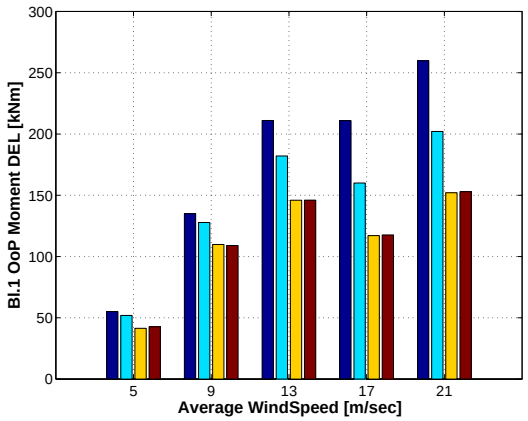

Figure 9. Blade nr.1 out–of–plane bending moment DEL as a function of wind intensity, computed from 600 sec simulations with turbulence intensity 8%. Columns from left to right: non–teetering reference control, non–teetering with multi–frequency MBML–based cyclic, teetering with reference control, teetering with cyclic control on teeter angle.

For the latter configuration the use of cyclic control provides a visible reduction also of this load, especially at lower speeds. On the other hand, cyclic control is largely ineffective in the teetering configuration, basically due to the different way loads are transferred to the shaft in this configuration, and the ensuing different dynamics of the rotor.

Figure 10 shows the top values of tip motion in the direction of the rotor axis, encountered on either of the two blades, as a function of wind. The value accounts for both the deformation and rigid motion, the latter being non–null only in the case of the teetering rotor. Considering the basic configurations without cyclic control, differently from the performance indices previously analyzed, the teetering rotor under this respect is generally far less advantageous than the non–teetering one.

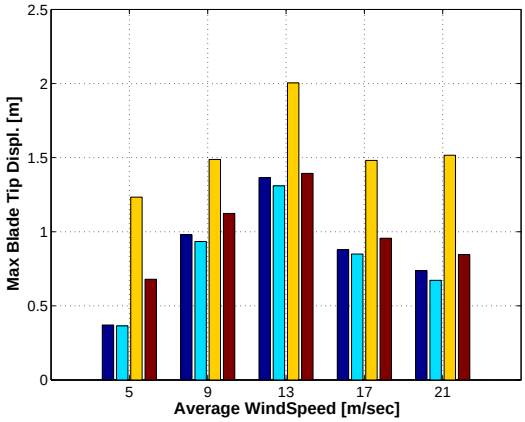

Figure 10. Maximum tip displacement in the direction of the rotor axis for the two blades as a function of wind intensity, computed from 600 sec simulations with turbulence intensity 8%. Columns from left to right: non–teetering reference control, non–teetering with multi–frequency MBML–based cyclic, teetering with reference control, teetering with cyclic control on teeter angle.

On the other hand, cyclic control is extremely effective in reducing the teeter motion of the teetering configuration, resulting in a top displacement which compares well with the top tip motion of the non–teetering rotor, which is only due to deformation. A comparatively lower effect is obtained from the use of cyclic control on the non–teetering rotor, which is actually operating on loads and not on a measure of blade motion, unlike the cyclic control in the teetering case.

The plot on Figure 11 shows both average power and the average–ratioed standard deviation of power – an index of power quality – as functions of the average wind. Values are normalized with respect to the results obtained on the non–teetering configuration with no cyclic control for all wind speeds, the corresponding column reading 1.0 at every speeds. Considering the two scenarios where cyclic control is not active, it is possible to note that the non–teetering configuration is clearly superior in terms of extracted power and power quality.

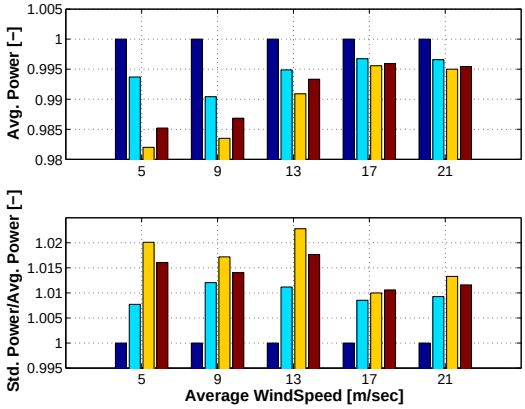

Figure 11. Normalized average power (top) and standard deviation of power ratioed by the average value, as functions of wind intensity, computed from 600 sec simulations with turbulence intensity 8%. Columns from left to right: non–teetering reference control, non–teetering with multi–frequency MBML–based cyclic, teetering with reference control, teetering with cyclic control on teeter angle.

As it is typical for load–targeting cyclic control also on three–bladed turbines, a certain reduction in average power with respect to the reference is obtained when activating cyclic control on a non–teetering turbine, while still remaining above the performance of the reference teetering machine. The use of cyclic control on the teetering rotor appears to improve significantly the performance of this configuration, increasing average power and reducing oscillations, reflected in the normalized standard deviation, especially in the partial power region.

DOI: 10.1002/we
Prepared using weauth.cls

4. CONCLUSIONS

In this work a novel transformation linking the harmonic content of blade and shaft signals has been described. The transformation can be applied to rotors with an arbitrary number of blades, with predictable relationships between input and output signals depending on the settings.

The derivation of the transformation for the specific case of two–bladed wind turbines has been presented thoroughly. For both teetering and non–teetering rotors, in ideal periodic conditions the proposed transformation, suitably configured, allows to obtain two signals in the fixed frame featuring a constant component with amplitudes equal to the cosine and sine components of the blade signals, and with the lowest polluting component at the 4P. Such frequency separation allows to use low–pass filters with a relatively wide band to treat the signals in the fixed system, thus making phase distortion a less relevant issue. The frequency separation effect is preserved in turbulence, making filter design easier also in a more realistic scenario.

In the case of non–teetering rotors, it has been shown how the transformed loads enable the use of a control law very similar to that usually adopted for three–bladed turbines, generating a cyclic pitch input able to effectively reduce harmonic loads on the blades. The transformation can be seamlessly reproduced at higher frequencies, thus allowing to promote higher harmonics in the blade signals to constants in the transformed signals. The latter can be treated to produce cyclic pitch components at the same frequency of the transformation. This in turn leads to an effective control action able to reduce higher harmonic components in the blade loads.

Due to the already satisfactory action of the passive control solution constituted by the implementation of a teeter pin, for teetering rotors the transformation has been used to target the teeter motion of the rotor instead of blade loads. The MBML–transformed teeter angle generates signals which, once fed to a control law basically identical to that considered for the non–teetering case, produce cyclic pitch components capable of effectively reducing blade tip motion and consequently increasing power production. Furthermore, it is expected that a more limited teeter motion would help reducing the chance of teeter end impacts and ensuing loads.

The control algorithms have been tested in a very realistic virtual environment on both teetering and non–teetering testbeds, leading to convincing results both in ideal normal wind profile (NWP) conditions and Cat. A or more typical 8% turbulence intensity (8% TI) winds, over all the operational spectrum of the machine.

In particular, for the non–teetering configuration the proposed control is able to substantially reduce loads on the blades and shaft, similar to what is obtained from a typical IPC on a three–bladed rotor. This comes at the expense of a negligible decrease in average power output and power quality.

The synergistic use of passive and active control on teetering rotors, provided respectively by the teeter hinge and the MBML individual pitch control, combines the best of both systems - as a result, the DEL on hub loads is almost annihilated, blade loads are abated, and at the same time the teeter motion is strongly reduced. In terms of power output, it can be observed that the teetering architecture is less advantageous with respect to a non–teetering one. The activation of the novel IPC controller mitigates this effect, increasing average power and also power quality with respect to a purely passive solution, over all the operating envelope of the machine.

Future work on the topic will include optimization techniques for automatic control parameters tuning aimed at performance refinement and balance, an investigation on the effect of teeter end through the application of the controller to a suitable machine, a full–scale envelope analysis in presence of the proposed control to study the effects on components design, testing on ad-hoc wind tunnel models and studying scaling effects on larger two–bladed wind turbines.

REFERENCES

1. Johnson, W., *Helicopter Theory*, Princeton University Press, Princeton, NJ, 1981.
2. Eggleston, DM, Stoddard, FS. *Wind Turbine Engineering Design*. Van Nostrand Reinhold, New York, NY, USA, 1987.
3. Bottasso, CL, Cacciola, S. Model-independent periodic stability analysis of wind turbines. *Wind Energy* 2014; **18**(5):865–887.
4. Johnson, W., "Self-Tuning Regulators for Multicyclic Control of Helicopter Vibration," NASA Technical Paper TP 1996, March 1982.
5. Bottasso, CL, Cacciola, S, Croce, A, Dozio, L. Load Reduction in Lead-Lag Dampers by Speed-Scheduled Aperture and Modulated Control of a Bypass Valve. *Journal of the American Helicopter Society* 2012; **57**(2):16-28.
6. Stol, KA. Disturbance tracking control and blade load mitigation for variable–speed wind turbines. *ASME Journal of Solar Energy Engineering*, 2003; **125**: 396–401.
7. Stol, KA, Balas, MJ. Periodic disturbance accommodating control for speed regulation of wind turbines. *ASME Journal of Solar Energy Engineering*, 2003;**125**: 379–385.
8. Bossanyi, E. Wind turbine control for load reduction. *Wind Energy* 2003; **6**: 229–244.

9. Bossanyi, E. Individual blade pitch control for load reduction. *Wind Energy* 2003; **6**: 119–128.
10. Bossanyi, E. Developments in individual blade pitch control. In *Proceedings of The Science of Making Torque from Wind Conference*, Delft, The Netherlands, 19–21 April 2004.
11. Bossanyi, E. Further load reductions with individual pitch control. *Wind Energy* 2005; **8**: 481–485.
12. Bottasso, CL, Croce, A, Riboldi, CED, Nam, Y. Multi–layer control architecture for the reduction of deterministic and non–deterministic loads on wind turbines. *Renewable Energy*, 2013; **51**: 159–169.
13. Bottasso, CL, Croce, A, Riboldi, CED, Salvetti, M. Cyclic pitch control for the reduction of ultimate loads on wind turbines. *Journal Of Physics Conference Series*, 2014; **524**(1), 012063.
14. Geyler, M, Caselitz, P. Individual blade pitch control design for load reduction on large wind turbines. In *Proceedings of the European Wind Energy Conference (EWEC 2007)*, Milano, Italy, 7–10 May 2007.
15. Van Engelen, TG, and Kanev, S. Exploring the limits in individual pitch control. In *Proceedings of the European Wind Energy Conference (EWEC 2009)*, Marseille, France, 16–19 March 2009.
16. Riboldi, CED. On the optimal tuning of individual pitch control for horizontal axis wind turbines. *Wind Engineering*, 2016; **40**: 398–416.
17. Riboldi, CED. Advanced control laws for variable speed wind turbines and supporting enabling technologies. PhD Thesis, 2012. Department of Aerospace Science and Technology, Politecnico di Milano, Italy. See also URL https://www.politesi.polimi.it.
18. Bossanyi, E, Wright, AD. Field testing of individual pitch control on the NREL CART–2 wind turbine. In *Proceedings of the European Wind Energy Conference (EWEC 2009)*, Marseille, France, 16–19 March 2009.
19. Schorbach, V, Haines, R, Dalhoff, P. Teeter end impacts: analysis and classification of most unfavourable events. *Wind Energy*, 2015; **19**(1): 115–121.
20. Bergami, L, Madsen, HA, Rasmussen, F. A two-bladed teetering hub configuration for the DTU 10 MW RWT: loads considerations. In *European Wind Energy Association Annual Event (EWEA 2014)*, Barcelona, Spain, 11–13 March 2014.
21. van Solingen, E, van Wingerden, JW. Linear individual pitch control design for two-bladed wind turbines. *Wind Energy* 2015; **18**(4):677–697.
22. van Solingen, E, Fleming, PA, Scholbrock, A, van Wingerden, JW. Field testing of linear individual pitch control on the two-bladed controls advanced research turbine. *Wind Energy* 2016; **19**(3):421–436.
23. Larsen, TJ, Madsen, HA, Thomsen, K, Rasmussen, F. Reduction of teeter angle excursions for a two-bladed downwind rotor using cyclic pitch control. In *European Wind Energy Conference and Exhibition (EWEC 2007)*, Milano, Italy, 7–10 May 2007.
24. Cacciola, S, Riboldi, CED. Equalizing aerodynamic blade loads through individual pitch control via multi–blade multi–lag transformation. *Journal of Solar Energy Engineering*, to appear 2017.
25. Bottasso, CL, Cacciola, S, Schreiber, J. A wake detector for wind farm control. *Journal of Physics: Conference Series*, 2015; **625**(1): 012007.
26. Jonkman, JM, Buhl, M. *FAST User's Guide*. National Renewable Energy Laboratory: Boulder, CO, 2005.
27. Bottasso, CL, Croce, A, Riboldi, CED, Nam, Y. Power curve tracking in the presence of a tip speed constraint. *Renewable Energy*, 2012; **40**: 1–12.
28. Many Authors, *IEC61400–1. Wind turbines – Part 1: design requirements*, 2006.

DOI: 10.1002/we
Prepared using weauth.cls